HAL
open science

The layered iron arsenide oxides Sr2CrO3FeAs and Ba2ScO3FeAs

Dirk Johrendt, Marcus Tegel, Franziska Hummel, Rainer Pöttgen, Inga Schellenberg, Sebastian Lackner

To cite this version:

Dirk Johrendt, Marcus Tegel, Franziska Hummel, Rainer Pöttgen, Inga Schellenberg, et al.. The layered iron arsenide oxides Sr2CrO3FeAs and Ba2ScO3FeAs. Journal of Inorganic and General Chemistry / Zeitschrift für anorganische und allgemeine Chemie, 2009, 635 (13-14), pp.2242. 10.1002/zaac.200900203 . hal-00492450

HAL Id: hal-00492450

https://hal.science/hal-00492450v1

Submitted on 16 Jun 2010

HAL is a multi-disciplinary open access archive for the deposit and dissemination of scientific research documents, whether they are published or not. The documents may come from teaching and research institutions in France or abroad, or from public or private research centers.

L'archive ouverte pluridisciplinaire **HAL**, est destinée au dépôt et à la diffusion de documents scientifiques de niveau recherche, publiés ou non, émanant des établissements d'enseignement et de recherche français ou étrangers, des laboratoires publics ou privés.

Zeitschrift für Anorganische und Allgemeine Chemie

The layered iron arsenide oxides Sr2CrO3FeAs and Ba2ScO3FeAs

Journal:	*Zeitschrift für Anorganische und Allgemeine Chemie*
Manuscript ID:	zaac.200900203
Wiley - Manuscript type:	Article
Date Submitted by the Author:	06-Apr-2009
Complete List of Authors:	Johrendt, Dirk; LMU Muenchen, Department Chemie und Biochemie Tegel, Marcus; LMU München, Chemie & Biochemie Hummel, Franziska; LMU München, Chemie & Biochemie Pöttgen, Rainer; Universität Münster, Anorganische Chemie Schellenberg, Inga; Universität Münster, Anorganische Chemie Lackner, Sebastian; Universität Münster, Anorganische Chemie
Keywords:	Iron arsenides, Superconductors, Crystal structure, Magnetism, Mössbauer spectroscopy

scholarONE™
Manuscript Central

The layered iron arsenide oxides Sr_2CrO_3FeAs and Ba_2ScO_3FeAs

Marcus Tegel[a], Franziska Hummel[a], Sebastian Lackner[a], Inga Schellenberg[b], Rainer Pöttgen[b], and Dirk Johrendt*[a]

[a] Department Chemie und Biochemie, Ludwig-Maximilians-Universität München, Butenandtstrasse 5–13 (Haus D), 81377 München, Germany

[b] Institut für Anorganische und Analytische Chemie, Westfälische Wilhelms-Universität Münster, Corrensstrasse 30, 48149 Münster, Germany

Abstract. The iron arsenide oxides Sr_2CrO_3FeAs and Ba_2ScO_3FeAs were synthesized by high temperature solid state reactions and their crystal structures determined by the X-ray powder diffraction. Their structures are tetragonal (*P*4/*nmm*; Sr_2CrO_3FeAs: a = 391.12(1) pm, c = 1579.05(3) pm; Ba_2ScO_3FeAs: a = 412.66(5) pm, c = 1680.0(2) pm, Z = 2) and isotypic to Sr_2GaO_3CuS. Iron arsenide layers are sandwiched between perowskite-like metal oxide layers and separated by ~1600 pm, which is much larger compared to the ZrCuSiAs-type '1111' iron arsenide superconductors. The bond lengths and angles within the FeAs layers are adapted to the space requirements of the oxide blocks. Measurements of the magnetic susceptibility, electrical resistivity and temperature-dependent crystal structure show no hint for a structural phase transition or magnetic anomaly in both compounds. Sr_2CrO_3FeAs shows Curie-Weiss paramagnetism above 160 K with an effective magnetic moment of 3.83(3) μ_B in good agreement with the theoretical value of 3.87 μ_B for Cr^{3+} (S = 3/2). Antiferromagnetic ordering was detected below T_N ~ 31 K. ^{57}Fe Mössbauer spectra of Sr_2CrO_3FeAs show one single signal that broadens below the Néel temperature due to a small transferred hyperfine field induced by the magnetic ordering of the chromium atoms. ^{57}Fe-Mössbauer spectra of Ba_2ScO_3FeAs show single signals which are only subject to weak quadrupole splitting.

Running title: Sr_2CrO_3FeAs and Ba_2ScO_3FeAs

Keywords: Iron arsenides, Superconductors, Crystal structure, Magnetism, ^{57}Fe Mössbauer-spectroscopy

*Prof. Dr. Dirk Johrendt
Department Chemie und Biochemie, Universität München
Butenandtstrasse 5–13 (Haus D), D-81377 München, Germany
e-mail: dirk.johrendt@cup.uni-muenchen.de

Introduction

The discovery of high-T_c superconductivity in iron arsenides [1] has generated an enormous and growing tide of interest [2], which is reflected in about 600 papers already published within one year. Besides outstanding superconducting properties with T_c's up to 55 K [3] and very high critical fields of at least 70 T [4], it is certainly also the richness of crystal chemical and physical properties, that has pushed this class of materials in the spotlight of interest.

Up to now, the family of iron-based superconductors consists of rather simple ternary or quaternary compounds with long known crystal structures, namely LaOFeAs with the ZrCuSiAs-type structure [1, 5], $BaFe_2As_2$ with $ThCr_2Si_2$-type structure [6-8], LiFeAs with PbFCl-type structure [9, 10] and β-FeSe with the anti-PbO structure [11, 12]. The currently by far most investigated compounds are the *RE*FeAsO ('1111', *RE* = rare earth) and AFe_2As_2 ('122', *A* = alkaline earth) based systems.

Superconductivity emerges in the FeAs layers built up by edge-sharing $FeAs_{4/4}$ tetrahedra, and is assumed to be unconventional [13, 14] because of the relatively high critical temperatures and the proximity to structural and magnetic transitions. The latter ones only occur in the non-superconducting 'parent compounds' like LaFeAsO [15] or $BaFe_2As_2$ [6] and have to be at least partially suppressed by doping or by external pressure before superconductivity arises [1, 8]. This scenario is reminiscent of the high-T_c cuprates, where also an antiferromagnetic ground-state of a layered parent compound like La_2CuO_4 becomes unstable upon doping before superconductivity appears [16]. However, this analogy is limited by the fact, that the doping of a Mott-insulator as in the case of the cuprates is of a very different nature compared to doping the metallic iron arsenides. Indeed, the metallic property of the parent compounds and the multi-band character of the Fermi-surfaces constitute significant differences between the cuprate and iron arsenide superconductors. It has also been shown that the anisotropy of the iron arsenide superconductors is significantly lower compared to the cuprates, which have even higher T_c's [17].

Even though one should be careful in transferring principles from the cuprates, it is an important task to search for new iron arsenides with lower dimensional structures, i. e. with larger FeAs interlayer distances. Several pnictide oxide structures are considerable candidates [18], but also materials derived form copper sulfide oxides with

isoelectronic CuS layers [19, 20] are very promising. The first reported compound was $Sr_3Sc_2O_5Fe_2As_2$ [21] with the known structure of $Sr_3Fe_2O_5Cu_2S_2$ [20]. The iron arsenide is not superconducting and shows no structural anomaly or magnetic ordering. Then superconductivity at 17 K [22] has been found in the iron phosphide Sr_2ScO_3FeP with the Sr_2GaO_3CuS-type [19] structure. This T_c is considerably higher in comparison with the ZrCuSiAs-Type phosphide oxides like LaFePO (4-7K) and may promise even higher *T*c's in analogue arsenides.

In this paper, we report on the iron arsenide oxides Sr_2CrO_3FeAs and Ba_2ScO_3FeAs, both sharing the key feature of tetragonal iron arsenide layers with other iron arsenide superconductors, but the interlayer distances are much larger due to separation by perowskite-like metal oxide blocks. Their crystal structures were determined by X-ray powder diffraction and the physical properties were characterized by magnetic susceptibility and electrical resistivity measurements and ^{57}Fe Mössbauer spectroscopy experiments. The electronic structure of the new compound Ba_2ScO_3FeAs is compared with the parent compounds of the superconducting iron arsenides.

Results

Crystal structure

The crystal structures of Sr_2CrO_3FeAs and Ba_2ScO_3FeAs are isotypic to the oxide sulfide Sr_2GaO_3CuS [19] in the space group *P*4/*nmm*. Figure 1 shows X-ray powder patterns, which could be completely fitted with one single phase in the case of Sr_2CrO_3FeAs using starting parameters from ref. [19]. Minor impurities of Sc_2O_3 and FeAs were detected in the Ba_2ScO_3FeAs sample. Crystallographic data, selected bond lengths and parameters of the Rietveld fits are compiled in Table 1. Further details of the structure determinations may be obtained from: Fachinformationszentrum Karlsruhe, D-76344 Eggenstein-Leopoldshafen (Germany) by quoting the Registry No's CSD-###### (Sr_2CrO_3FeAs) and CSD-###### (Ba_2ScO_3FeAs).

The crystal structure of Sr_2CrO_3FeAs and Ba_2ScO_3FeAs is shown in Figure 2. The FeAs layers perpendicular to the *c*-axis are separated by strontium atoms from chromium oxide and strontium oxide layers according to the stacking order $(CrO_2)(SrO)(SrO)(CrO_2)$. The Fe–As bonds are shorter and the $FeAs_{4/4}$ tetrahedra are

less distorted in Sr_2CrO_3FeAs in comparison with Ba_2ScO_3FeAs. Also the Fe–Fe distance is significantly shorter in the strontium compound (276.6 pm) than in the barium compound (291.8 pm). This may be attributed to the larger required space of the barium ions and to a smaller extent the scandium ions, and it shows that the geometry of the FeAs layer is flexible and can be adapted to the oxide blocks. The interlayer distance of the iron arsenide layers equals the *c* lattice parameter for this structure type, thus Ba_2ScO_3FeAs (c = 1680 pm) exhibits the highest iron arsenide interlayer distance so far. The powder patterns recorded at lower temperatures revealed no structural phase transitions for both compounds down to 10 K. At 10 K, the corresponding *a* lattice parameter is decreased by 0.73 pm (0.92 pm) and the *c* lattice parameter by 8.4 pm (6.0 pm) for Sr_2CrO_3FeAs (Ba_2ScO_3FeAs).

Magnetism and resistivity

Figure 3 shows the magnetic susceptibility of Sr_2CrO_3FeAs between 1.8 and 360 K. The compound obeys the Curie-Weiss law above ~ 160 K. An effective magnetic moment of 3.83(3) μ_B was found, which is in good agreement with the theoretical spin-only value of 3.87 μ_B for Cr^{3+} (S = 3/2). The paramagnetic temperature is –141(3) K. Antiferromagnetic ordering is discernible, the highest susceptibility was reached at T_N ~ 31 K. The origin of the anomaly around 120 K is not yet clear, but probably due to traces of ferromagnetic contamination. Ba_2ScO_3FeAs is Pauli-paramagnetic in the temperature range between 1.8 and 300 K (not shown). Neither compound shows any sign of anomaly in the course of the magnetic susceptibility at any applied external magnetic field. The resistivity of both Sr_2CrO_3FeAs and Ba_2ScO_3FeAs is depicted in Figure 4. Both compounds are poor metals over the whole measured temperature range and show no anomaly. Both magnetism and resistivity therefore indicate that there is no occurrence of a spin-density-wave anomaly in any of the compounds.

Mößbauer spectroscopy

The ^{57}Fe Mössbauer spectra collected for the Sr_2CrO_3FeAs sample at various temperatures are shown in Figure 5 together with transmission integral fits. The corresponding fitting parameters are summarized in Table 2. As expected from the crystal structure (one single Fe site), the spectra at 298, 77, and 40 K are well

reproduced with single signals, which are subject to weak quadrupole splitting due to the non-cubic site symmetry (4;$^{\bar{}}m2$) of the iron atoms. Within the standard deviations, the observed isomer shift, the experimental line width, and the quadrupole splitting of Sr_2CrO_3FeAs are almost identical with those obtained for $Sr_3Sc_2O_5Fe_2As_2$ [23], indicating a similar electronic situation for the iron atoms in both arsenide oxides. The observed isomer shift is in line with the recently reported ^{57}Fe data for LaFePO [24], $SrFe_2As_2$ [25], and $BaFe_2As_2$ [26]. The increase of the isomer shift with decreasing temperature (0.29 → 0.45 mm/s) is due to a second order Doppler shift (SODS), well known for iron compounds.

In contrast to $Sr_3Sc_2O_5Fe_2As_2$ [21], where no magnetic ordering is observed down to 4.2 K, the chromium atoms in Sr_2CrO_3FeAs reveal antiferromagnetic ordering. This is also reflected in the ^{57}Fe Mössbauer spectra at 20 and 4.2 K, i. e. well below the Néel temperature. In the magnetically ordered regime we observe significant broadening of the Mössbauer signal and the fits revealed increased line width and quadrupole splitting parameters. Since the transferred field (B_{hf}) is small, independent refinement of all parameters, δ, Γ, ΔE_Q, and B_{hf} showed strong correlations. In order to get an estimate for the transferred field, the 4.2 K spectrum was fitted with various fixed values for the hyperfine field. A reasonable fit was obtained for a fixed hyperfine field of 0.5 T and the refined values δ = 0.45(1) mm/s, Γ = 0.84(2) mm/s, and ΔE_Q = 0.24(1) mm/s. From these fitting tests we estimate a transferred hyperfine field of 0.5±0.2 T at 4.2 K.

Figure 6 shows the ^{57}Fe Mössbauer spectra of the Ba_2ScO_3FeAs sample at various temperatures together with transmission integral fits. The fitting parameters are listed in Table 2. In agreement with the single Fe site in the crystal structure, the spectra at 298, 77, and 4.2 K show single signals which are subject to weak quadrupole splitting. The 77 K isomer shifts of Ba_2ScO_3FeAs (Table 2), $Sr_3Sc_2O_5Fe_2As_2$ [23], and Sr_2CrO_3FeAs are almost identical. We can thus assume a similar electronic situation within the tetrahedral [Fe_2As_2] layers of the three structures. They are also comparable to LaFePO [24] and $SrFe_2As_2$ [25]. The increase of the isomer shift with decreasing temperature (0.35 → 0.50 mm/s) results from a second order Doppler shift. The spectra give no hint for magnetic ordering of the iron moments down to 4.2 K. Ba_2ScO_3FeAs and $Sr_3Sc_2O_5Fe_2As_2$ show a lower quadrupole splitting parameter (0.20 mm/s for both compounds) than Sr_2CrO_3FeAs (0.42 mm/s) at 4.2 K. Even smaller values of ΔE_Q = 0.19 and -0.04 mm/s occur for LaFePO and $BaFe_2As_2$, respectively.

Electronic structure

The electronic structure of the iron arsenide superconductors have frequently been described [27-31] and some (maybe hidden) electronic order with respect to superconductivity is still under discussion [32]. Also $Sr_3Sc_2O_5Fe_2As_2$ and the superconducting phosphide Sr_2ScO_3FeP have been studied recently [33,34]. In all cases, the calculations predict a Fermi surface consisting of hole-like pockets at the center of the Brillouin zone (Γ) and similar electron-like pockets at the corners (M), which become largely congruent by a vector (π,π). This Fermi surface nesting is an unstable situation and typically favors charge- or spin-density ordering, often connected with structural distortions. We have calculated the band structure of Ba_2ScO_3FeAs in order to see whether the rather large metal oxide building blocks between the FeAs layers induces any appreciable perturbance of the bands close to the Fermi level and thus the Fermi surface. The band structure of Ba_2ScO_3FeAs (Figure 7, top) shows the typical features known from the iron arsenide superconductors [27]. Iron 3*d* band contributions (emphasized in Figure 7) clearly dominate the vicinity of the Fermi level, where no significant contributions of the oxide layers are found. Also the Fermi surface (Figure 7, bottom), reveals the typical cylinders around Γ and M and provides the unstable nesting situation as mentioned above. Thus from the view of the electronic structure, one would expect structural and magnetic anomalies in Ba_2ScO_3FeAs. The origin of the absence of any structural or magnetic instability and superconductivity in this and the related compounds is not clear and currently under investigation.

Conclusion

The iron arsenide oxides Sr_2CrO_3FeAs and Ba_2ScO_3FeAs crystallize in the tetragonal Sr_2GaO_3CuS-type structure (space group *P*4/*nmm*) and exhibit the largest distance between the FeAs layers so far due to separation by large perowskite-like metal oxide blocks. The chromium compound shows paramagnetism in agreement with Cr^{3+} (S = 3/2) and antiferromagnetic ordering below 31 K, whereas Ba_2ScO_3FeAs is Pauli-paramagnetic. Both compounds are poor metals and show no structural or magnetic anomalies, even though the electronic structure predicts a nested Fermi surface. ^{57}Fe-Mössbauer spectra are in agreement with the absence of magnetic ordering at the iron

site. In the case of Sr_2CrO_3FeAs, a small hyperfine field is transferred to the iron nuclei from the adjacent magnetically ordered CrO_2 layers.

Note added: While we were finalizing our manuscript, we recognized an unpublished manuscript by H. Ogino et al. [35]. Therein, the iron arsenide oxides Sr_2MO_3FeAs (M = Sc, Cr) are reported. The resistivity and susceptibility data are slightly different from our results.

Acknowledgments

We thank Dipl.-Chem. Bele Boeddinghaus and Prof. Thomas Fässler for help with the magnetic measurements. This work was financially supported by the Deutsche Forschungsgemeinschaft.

Experimental

Synthesis

Sr_2CrO_3FeAs and Ba_2ScO_3FeAs were synthesized by heating stoichiometric mixtures of strontium, chromium, iron (III) oxide, arsenic oxide and barium, scandium, iron (III) oxide and arsenic oxide, respectively in alumina crucibles sealed in silica ampoules under an atmosphere of purified argon. The mixtures were heated to 1323 K at a rate of 80 K/h, kept at this temperature for 60 h and cooled down to room temperature. The products were homogenized in an agate mortar, pressed into pellets and sintered at 1323 K for 60 h, reground, pressed into pellets and sintered again at 1323 K for 50 h.

Crystal structure determination

Powder patterns were recorded on STOE STADI P Debye-Scherrer X-Ray diffractometers (Mo-$K_{\alpha 1}$ and Cu-$K_{\alpha 1}$ radiation, respectively, Ge-111 monochromator, Debye-Scherrer or transmission geometry). Rietveld refinements of both samples were performed with the TOPAS package [36] using the fundamental parameters approach as

reflection profiles (convolution of appropriate source emission profiles with axial instrument contributions as well as crystallite microstructure effects). In order to describe small peak half width and shape anisotropy effects, the approach of *Le Bail* and *Jouanneaux* [37] was implemented into the TOPAS program and the according parameters were allowed to refine freely. Preferred orientation of the crystallites was described with a spherical harmonics function of 4th or 8th order. In order to check for structural phase transitions, powder patterns between 10 and 300 K were recorded on a Huber G670 Guinier imaging plate diffractometer (Cu-$K_{\alpha 1}$ radiation, Ge-111 monochromator), equipped with a closed-cycle He-cryostat. These patterns were also refined with the TOPAS package using the approach described in Ref. [26].

Resistivity measurements

Sintered powder pellets (diameter = 6 mm, height ≈ 1.4 mm) of the samples were contacted with copper wires and silver conducting paint, and the electrical resistivity was measured between 10 and 320 K using a dc four-point current-reversal method [38].

Magnetic measurements

The magnetic properties were studied using a commercial SQUID magnetometer (Quantum Design MPMS-5) with external magnetic fields up to 50 kOe. Susceptibilities were measured at 100, 500, 1000, 5000 and 10000 Oe and hysteresis loops were taken at various temperatures to check for ferromagnetic ordering or impurity phases.

^{57}Fe Mössbauer spectroscopy

A ^{57}Co/Rh source was available for the ^{57}Fe Mössbauer spectroscopy investigations. The quoted values of the isomer shifts are given relative to this material. The $Sr_3Sc_2O_5Fe_2As_2$ sample was placed in a thin-walled PVC container. The measurements were conducted in the usual transmission geometry at temperatures between 4.2 and 298 K. The source was kept at room temperature. The total counting time was 1 day per spectrum. Fitting of the spectra was carried out with the NORMOS-90 program system [39].

Computational details

Electronic structure calculations for Ba_2ScO_3FeAs were performed with the *WIEN2k* program package [40] using density functional theory within the full-potential *LAPW* method and the local density approximation (*LDA*). Detailed descriptions for both methods are given elsewhere [41]. Full-potential *LAPW*, which was used for the *WIEN2k* calculations, is based on the muffin-tin construction with non-overlapping spheres. In the interstitial region between spheres, the potential is represented by a plane wave expansion. Because of the great flexibility and accuracy of this expansion for the potential and charge density, a very high numerical accuracy is achieved for the *LAPW* method. Mixed *LAPW* and *APW* + *lo* (*lo* = local orbitals) basis sets were used to increase the efficiency of the *APW* linearization [42]. Further technical details can be found in ref. [43] and the monograph of Singh [44]. The total energies and charge densities of the SCF cycles converged to changes smaller than 1×10^{-4} Ryd cell^{-1} and 4374 *k*-points ($27 \times 27 \times 6$ mesh) were used in the irreducible wedges of the Brillouin zones. The basis sets consisted of 4192 plane waves up to a cutoff $R_{mt}K_{max} = 8.0$. The atomic sphere radii R_{mt} were 2.50 (Ba), 1.97 (Sc), 2.43 (Fe), 2.16 (As) and 1.75 au (O). Fermi surfaces were visualized with XCrysDen [45].

References

[1] Y. Kamihara, T. Watanabe, M. Hirano, H. Hosono, *J. Am. Chem. Soc.* **2008**, *130*, 3296.

[2] D. Johrendt, R. Pöttgen, *Angew. Chem. Int. Ed.* **2008**, *47*, 4782.

[3] Z.-A. Ren, W. Lu, J. Yang, W. Yi, X.-L. Shen, Z.-C. Li, G.-C. Che, X.-L. Dong, L.-L. Sun, F. Zhou, Z.-X. Zhao, *Chin. Phys. Lett.* **2008**, *25*, 2215.

[4] J. D. Corbett, *J. Solid State Chem.* **1981**, *37*, 335.

[5] V. Johnson, W. Jeitschko, *J. Solid State Chem.* **1974**, *11*, 161.

[6] M. Rotter, M. Tegel, I. Schellenberg, W. Hermes, R. Pöttgen, D. Johrendt, *Phys. Rev. B* **2008**, *78*, 020503(R).

[7] M. Pfisterer, G. Nagorsen, *Z. Naturforsch. B - Chem. Sci.* **1980**, *35B*, 703.

[8] M. Rotter, M. Tegel, D. Johrendt, *Phys. Rev. Lett.* **2008**, *101*, 107006.

[9] R. Juza, K. Langer, *Z. Anorg. Allg. Chem.* **1968**, *361*, 58.

[10] J. H. Tapp, Z. J. Tang, B. Lv, K. Sasmal, B. Lorenz, P. C. W. Chu, A. M. Guloy, *Phys. Rev. B* **2008**, *78*.

[11] F. C. Hsu, J. Y. Luo, K. W. Yeh, T. K. Chen, T. W. Huang, P. M. Wu, Y. C. Lee, Y. L. Huang, Y. Y. Chu, D. C. Yan, M. K. Wu, *Proc. Natl. Acad. Sci. U. S. A.* **2008**, *105*, 14262.

[12] G. Hägg, A. L. Kindström, *Z. Phys. Chem. B* **1933**, *22*, 453.

[13] L. Shan, Y. L. Wang, X. Y. Zhu, G. Mu, L. Fang, C. Ren, H. H. Wen, *Europhys. Lett.* **2008**, *83*, 57004.

[14] A. D. Christianson, E. A. Goremychkin, R. Osborn, S. Rosenkranz, M. D. Lumsden, C. D. Malliakas, I. S. Todorov, H. Claus, D. Y. Chung, M. G. Kanatzidis, R. I. Bewley, T. Guidi, *Nature* **2008**, *456*, 930.

[15] C. d. l. Cruz, Q. Huang, J. W. Lynn, J. Li, W. RatcliffII, J. L. Zarestky, H. A. Mook, G. F. Chen, J. L. Luo, N. L. Wang, P. Dai, *Nature* **2008**, *453*, 899.

[16] J. G. Bednorz, K. A. Mueller, M. Takashige, *Science* **1987**, *236*, 73.

[17] N. Ni, S. L. Bud'ko, A. Kreyssig, S. Nandi, G. E. Rustan, A. I. Goldman, S. Gupta, J. D. Corbett, A. Kracher, P. C. Canfield, *Phys. Rev. B* **2008**, *78*, 014507.

[18] T. C. Ozawa, S. M. Kauzlarich, *Sci. Technol. Adv. Mater.* **2008**, *9,* 033003.

[19] W. J. Zhu, P. H. Hor, *Inorg. Chem.* **1997**, *36*, 3576.

[20] W. J. Zhu, P. H. Hor, *J. Solid State Chem.* **1997**, *134*, 128.

[21] X. Zhu, F. Han, G. Mu, B. Zeng, P. Cheng, B. Shen, and H.-H.Wen, *Phys Re*v. *B* **2009**, *79*, 024516.

[22] H. Ogino, Y. Matsumura, Y. Katsura, K. Ushiyama, S. Horii, K. Kishio, J.-J. Shimoyama, *arXiv*:0903.3314 (unpublished).

[23] M. Tegel, I. Schellenberg, R. Pöttgen, D. Johrendt, *Z. Naturforsch. B – Chem. Sci.* **2009**, submitted.

[24] M. Tegel, I. Schellenberg, R. Pöttgen, D. Johrendt, *Z. Naturforsch. B – Chem. Sci.* **2008**, *63*, 1057.

[25] M. Tegel, M. Rotter, V. Weiss, F. Schappacher, R. Pöttgen, D. Johrendt, *J. Phys.: Condens. Matter* **2008**, *20*.

[26] M. Rotter, M. Tegel, I. Schellenberg, F. M. Schappacher, R. Pöttgen, J. Deisenhofer, A. Gunther, F. Schrettle, A. Loidl, D. Johrendt, *New J. Phys.* **2009**, *11*.

[27] D. J. Singh, M. H. Du, *Phys. Rev. Lett.* **2008**, *100*, 237003.

[28] K. Haule, J. H. Shim, G. Kotliar, *Phys. Rev. Lett.* **2008**, *100*, 226402.

[29] G. Xu, H. J. Zhang, X. Dai, Z. Fang, *Europhys. Lett.* **2008**, *84*, 67015.

[30] D. J. Singh, *Phys. Rev. B* **2008**, *78*, 094511.

[31] I. A. Nekrasov, Z. V. Pchelkina, M. V. Sadovskii, *JETP Letters* **2008**, *88*, 144.

[32] V. B. Zabolotnyy, D. S. Inosov, D. V. Evtushinsky, A. Koitzsch, A. A. Kordyuk, G. L. Sun, J. T. Park, D. Haug, V. Hinkov, A. V. Boris, C. T. Lin, M. Knupfer, A. N. Yaresko, B. Büchner, A. Varykhalov, R. Follath, S. V. Borisenko, *Nature* **2009**, *457*, 569.

[33] I. R. Shein, A. L. Ivanovskii, *JETP Lett.* **2009**, *89*, 41.

[34] I. R. Shein, A. L. Ivanovskii, *arXiv*:0904.0117 (unpublished)

[35] H. Ogino, Y. Matsumura, Y. Katsura, K. Ushiyama, S. Horii, K. Kishio, J. Shimoyama, *arXiv*:0903.5124 (unpublished).

[36] A. Coelho, *TOPAS-Academic, version 4.1, Coelho Software*, Brisbane, **2007**.

[37] A. Le Bail, Jouanneaux, *J. Appl. Crystallogr.* **1997**, *30*, 265.

[38] KEITHLEY, *Low Level Measurements, Precision DC Current, Voltage and Resistance Measurements*, 5 ed., Keithley Instruments, Inc., Cleveland, Ohio, **1998**.

[39] R. A. Brand, *NORMOS Mössbauer fitting Program*, Universität Dortmund, **2002**.

[40] P. Blaha, K. Schwarz, G. K. H. Madsen, D. Kvasnicka, J. Luitz, 6 ed., TU Wien, **2001**.

[41] K. Schwarz, P. Blaha, *Comput. Mat. Sci.* **2003**, *28*, 259.

[42] E. Sjostedt, L. Nordstrom, D. J. Singh, *Solid State Commun.* **2000**, *114*, 15.

[43] G. K. H. Madsen, P. Blaha, K. Schwarz, E. Sjostedt, L. Nordstrom, *Phys. Rev. B* **2001**, *64*, 195134/1.

[44] D. J. Singh, L. Nordstrom, *Planewaves, Pseudopotentials and the LAPW Method*, Springer, New York, **2006**.

[45] A. Kokalj, *Comp. Mat. Sci.* **2003**, *28*, 155.

Tables

Table 1. Crystallographic data for Sr_2CrO_3FeAs and Ba_2ScO_3FeAs at 297 K.

compound	Sr_2CrO_3FeAs	Ba_2ScO_3FeAs
space group	*P*4/*nmm* (*o*2)	*P*4/*nmm* (*o*2)
molar mass (g mol^{-1})	406.001	498.375
lattice parameters (pm)	*a* = 391.12(1)	*a* = 412.66(5)
	c = 1579.05(3)	*c* = 1680.0(2)
cell volume, (nm^3)	0.24156(1)	0.28608(7)
density, (g cm^{-3})	5.582(1)	5.786(1)
μ (mm^{-1})	76.869	25.109
Z	2	2
data points	9600	5350
reflections (main phase)	108	259
d range	1.003 – 15.790	0.7631 – 16.800
atomic variables	13	12 (1 constraint)
profile variables	5	5
anisotropy variables	12	24
background variables	48	48
variables of impurity phases	0	20
other variables	8	12
R_P, wR_P	0.014, 0.018	0.036, 0.047
R_{bragg}, χ^2	0.002, 0.969	0.008, 1.186
wght. Durbin-Watson *d* stat.	1.707	1.140
Atomic parameters:		
Sr1/Ba1	2*c* (¾, ¾, *z*); *z* = 0.1957(2); U_{iso} = 83(5)	2*c* (¾, ¾, *z*); *z* = 0.1860(1); U_{iso} = 163(6)
Sr2/Ba2	2*c* (¾, ¾, *z*); *z* = 0.4150(1); U_{iso} = 98(7)	2*c* (¾, ¾, *z*); *z* = 0.4145(1); U_{iso} = 129(6)
Cr1/Sc1	2*c* (¼, ¼, *z*); *z* = 0.3108(2); U_{iso} = 88(9)	2*c* (¼, ¼, *z*); *z* = 0.3092(4); U_{iso} = 61(14)
Fe1	2*a* (¼, ¾, 0); U_{iso} = 77(8)	2*a* (¼, ¾, 0); U_{iso} = 190(11)
As1	2c (¼, ¼, *z*); *z* = 0.0899(2); U_{iso} = 79(8)	2c (¼, ¼, *z*); *z* = 0.0777(2); U_{iso} = 103(11)
O1	4*f* (¼, ¾, *z*); *z* = 0.2931(4); U_{iso} = 78(22)	4*f* (¼, ¾, *z*); *z* = 0.2898(7); U_{iso} = 262(32)
O2	2*c* (¼, ¼, *z*); *z* = 0.4313(6); U_{iso} = 88(30)	2*c* (¼, ¼, *z*); *z* = 0.427(1); U_{iso} = 262(32)
Selected bond lengths (pm) and angles (degrees):		
Sr/Ba – O	242.7(9)×1; 248.8(4)×4;	266(2)×1; 270.2(8)×4;
	274.4(5)×4; 277.8(1)×4	292.6(2)×4; 294.0(9)×4
Cr/Sc – O	190(1)×1; 197.5(1)×4	198(2)×1; 208.9(2)×4
Fe – Fe	276.6(1)×4	291.8(1)×4
Fe – As	241.7(2)×4	244.1(2)×4
As – Fe – As	110.2(1)×4; 108.0(1)×2	106.6(1)×4; 115.4(1)×2
O – Cr/Sc – O	88.9(1)×4; 98.1(2)×4; 163.7(4)×2	88.6(1)×4; 99.0(4)×4; 162.1(7)×2

Table 2. Fitting parameters of ^{57}Fe Mössbauer spectra at different temperatures. Γ: experimental line width, δ: isomer shift; ΔE_Q: electric quadrupole splitting parameter (for details see text).

Sr_2CrO_3FeAs

T / K	Γ / mms^{-1}	δ / mms^{-1}	ΔE_Q / mms^{-1}
298	0.37(1)	0.29(1)	0.22(1)
77	0.36(1)	0.42(1)	0.24(1)
40	0.31(1)	0.43(1)	0.23(1)
20	0.48(1)	0.43(1)	0.28(1)
4.2	0.67(2)	0.45(1)	0.43(1)

Ba_2ScO_3FeAs

T / K	Γ / mms^{-1}	δ / mms^{-1}	ΔE_Q / mms^{-1}
298	0.39(1)	0.35(1)	0.21(1)
77	0.45(1)	0.47(1)	0.20(1)
4.2	0.43(2)	0.50(1)	0.20(1)

Figure Captions

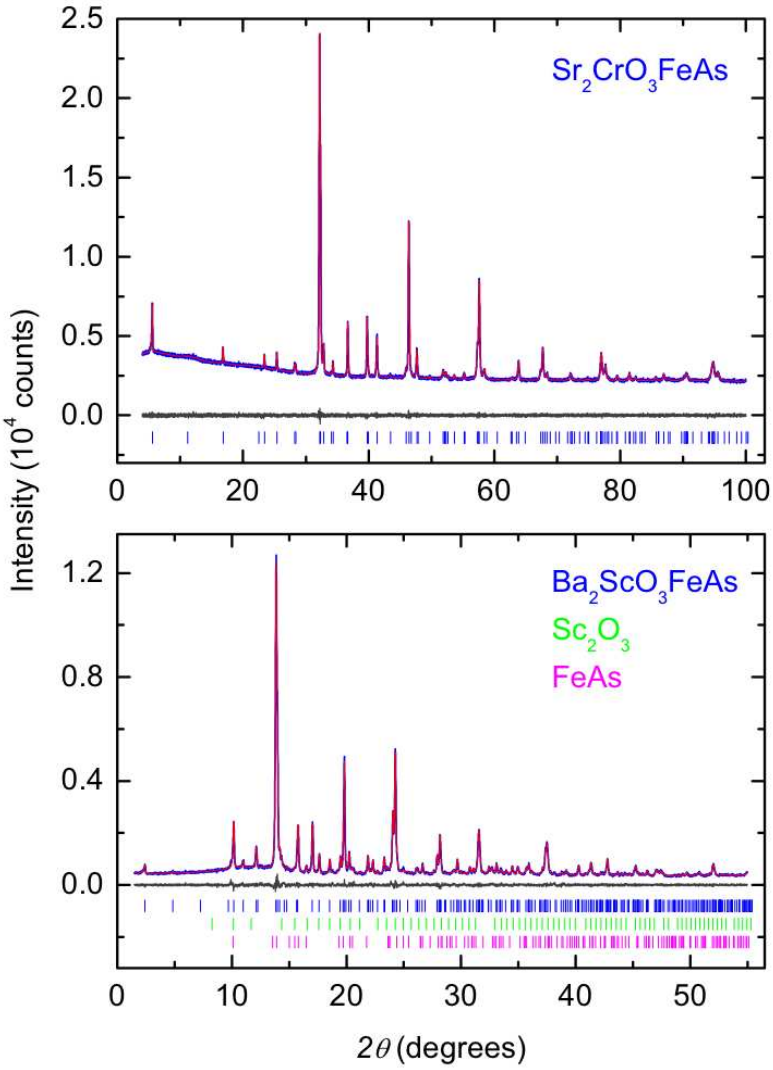

Fig. 1. Powder pattern (blue) and Rietveld fit (red) of Sr_2CrO_3FeAs and Ba_2ScO_3FeAs at 297 K (space group *P*4/*nmm*). Bottom: Sc_2O_3 and FeAs were included in the refinement as minor impurity phases.

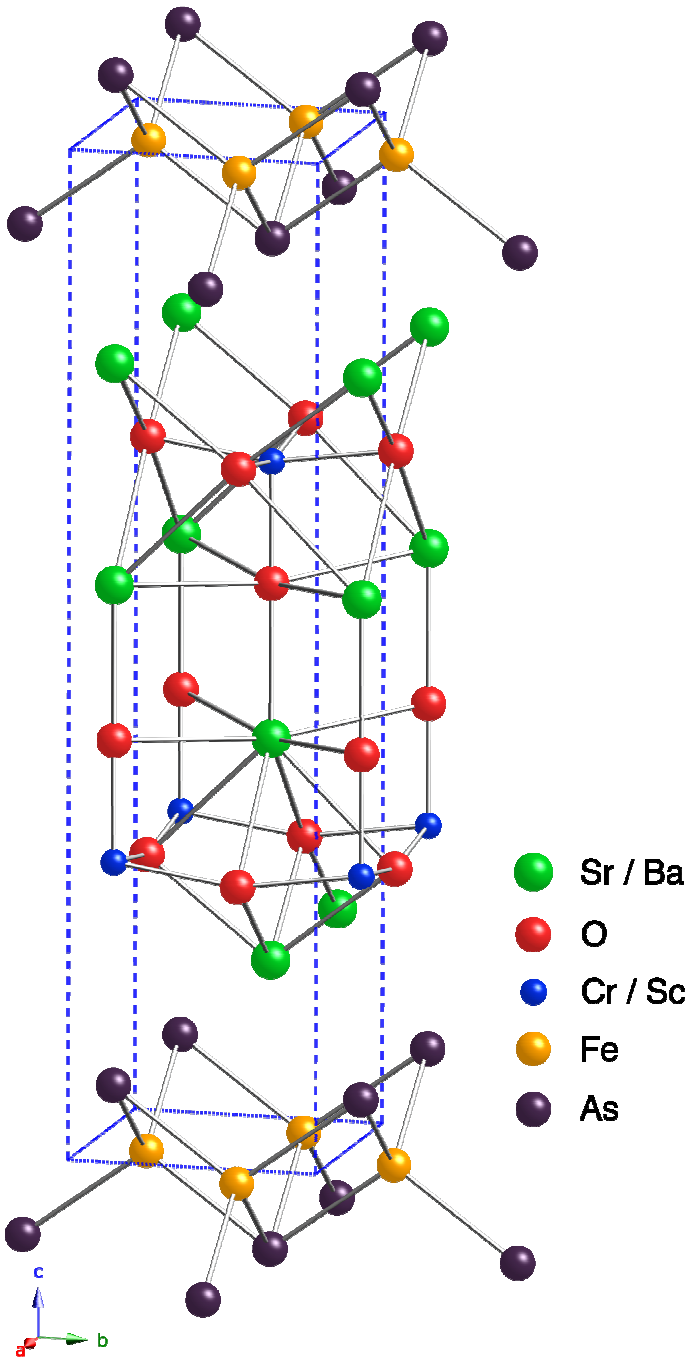

Fig. 2. The crystal structure of Sr_2CrO_3FeAs and Ba_2ScO_3FeAs.

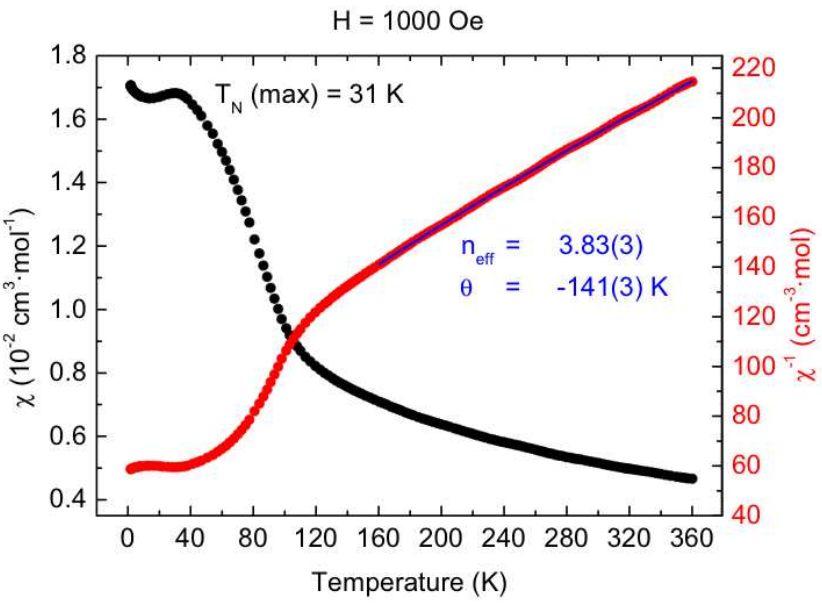

Fig. 3. Magnetic susceptibility (black), inverse susceptibility (red) and Curie-Weiss fit (blue) of Sr_2CrO_3FeAs.

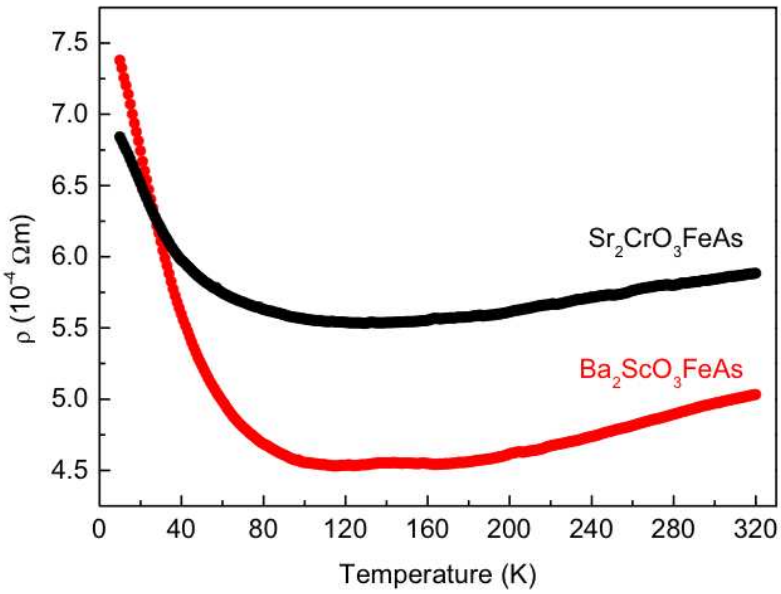

Fig. 4. Resistivity of Sr_2CrO_3FeAs (black) and Ba_2ScO_3FeAs (red).

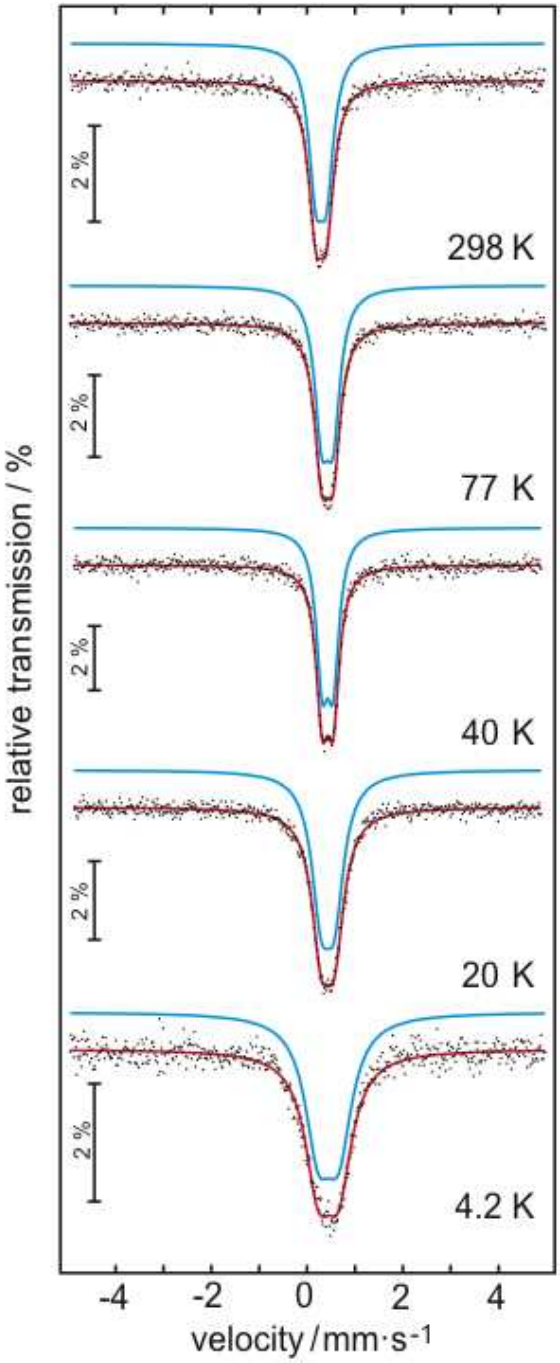

Fig. **5.** Experimental and simulated ^{57}Fe Mössbauer spectra of Sr_2CrO_3FeAs at various temperatures.

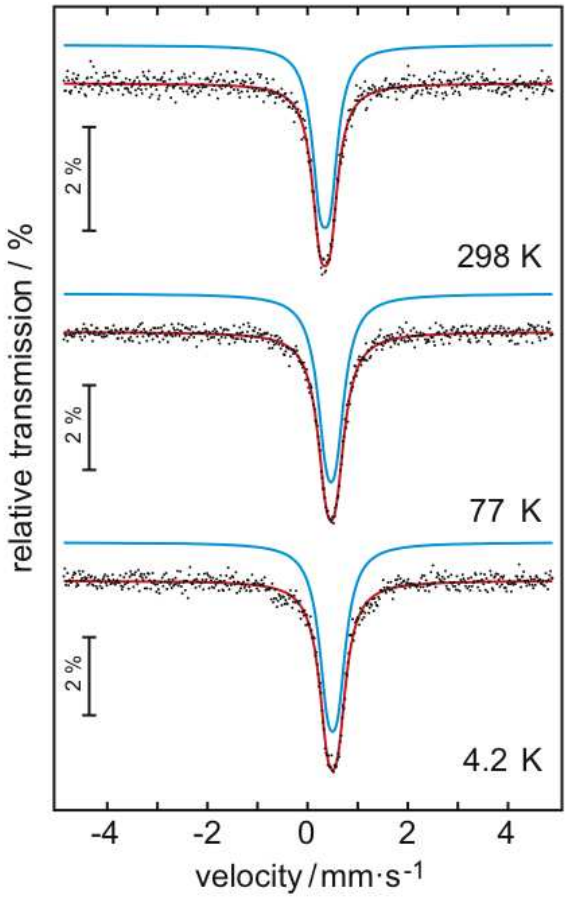

Fig. 6. Experimental and simulated ^{57}Fe Mössbauer spectra of Ba_2ScO_3FeAs at various temperatures.

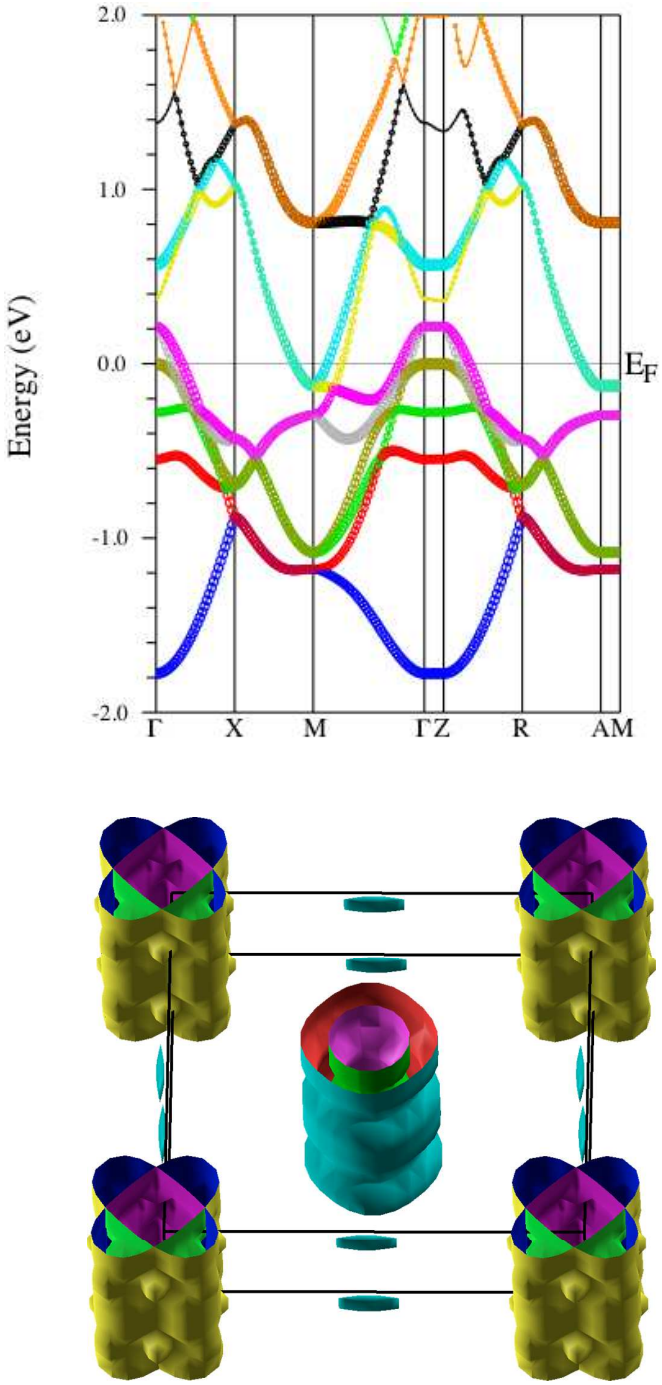

Figure 7. Top: Band structure of Ba_2ScO_3FeAs with the iron 3*d* contributions emphasized. Bottom: The Fermi surface showing the typical cylinders around the center (Γ, hole-like) and the corners (*M*, electron-like).

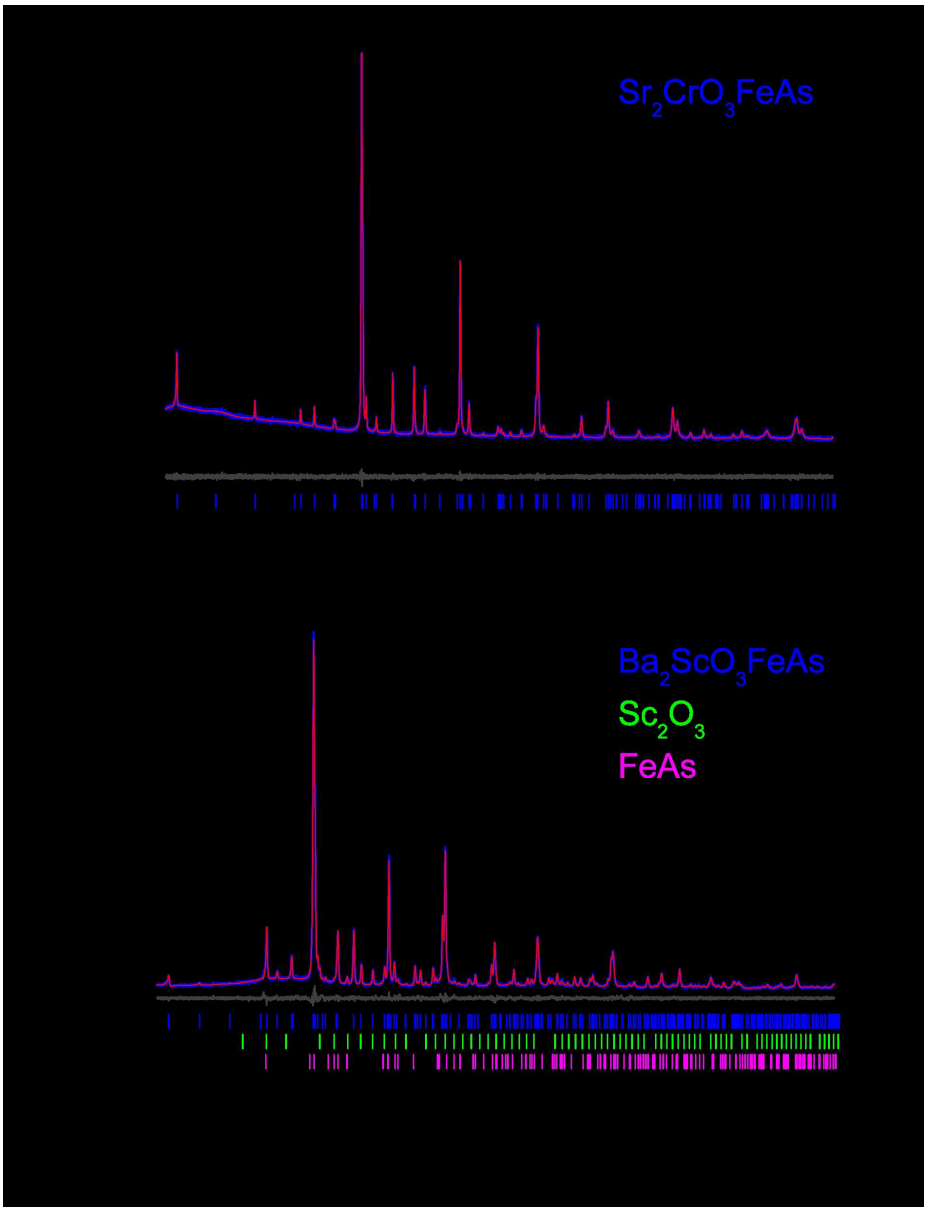

80x104mm (600 x 600 DPI)

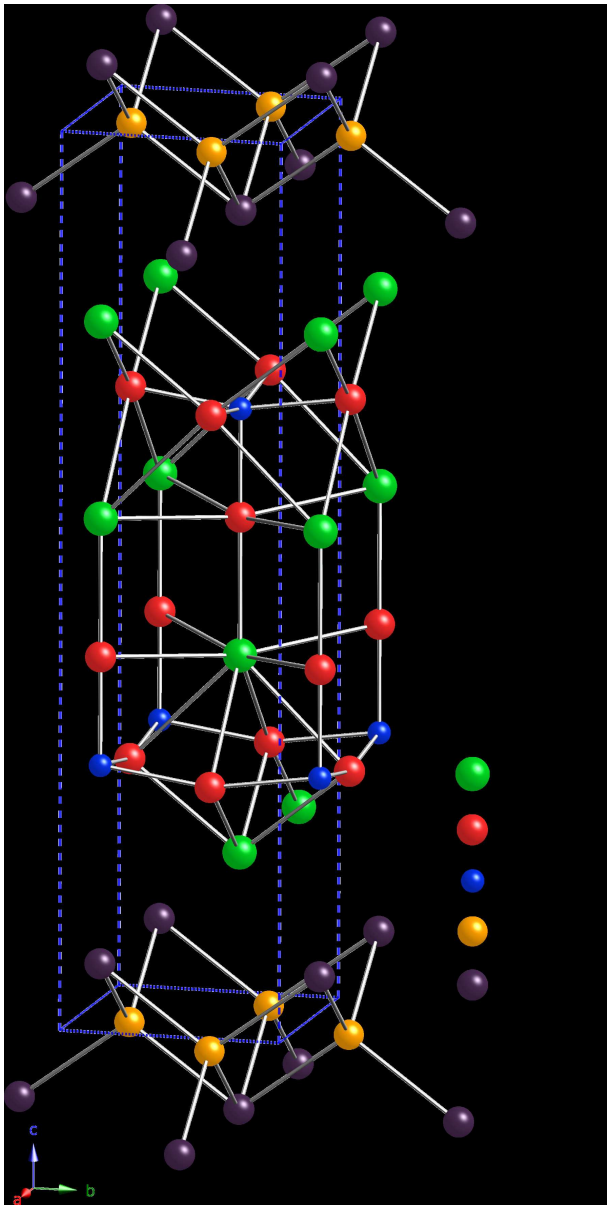

75x149mm (600 x 600 DPI)

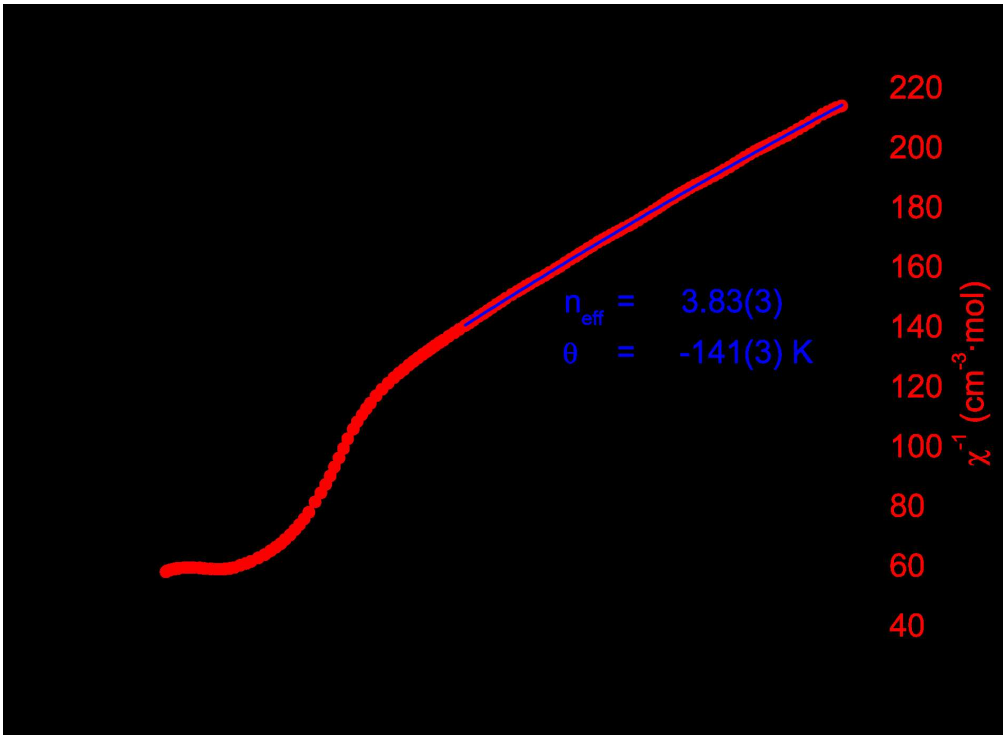

80x58mm (600 x 600 DPI)

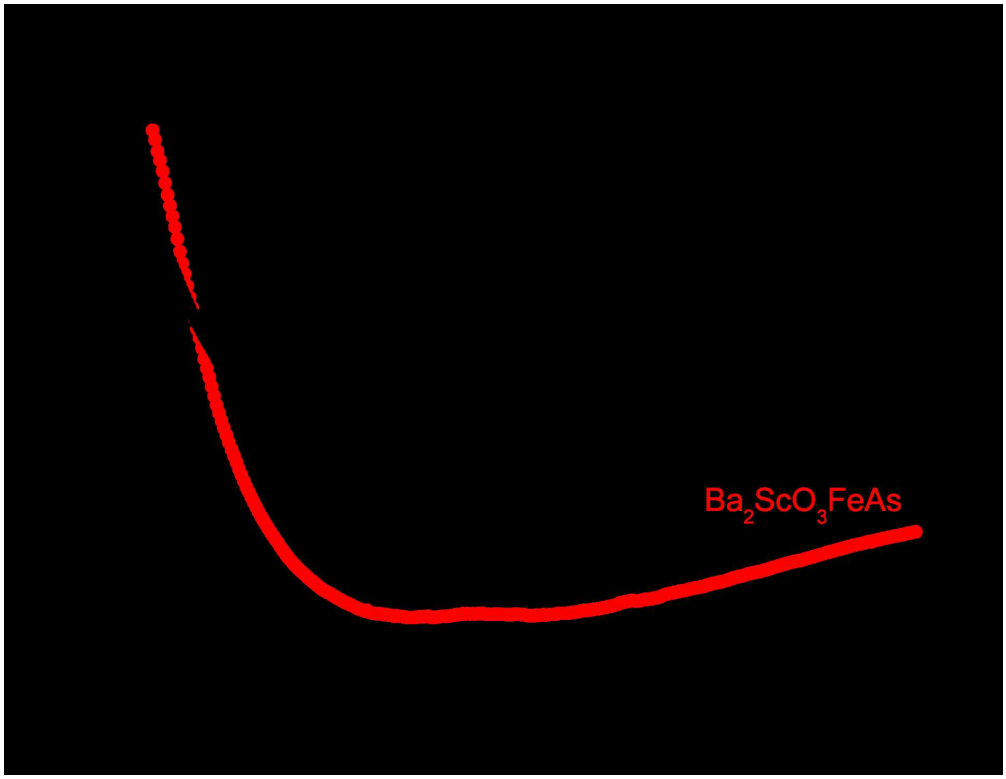

80x61mm (600 x 600 DPI)

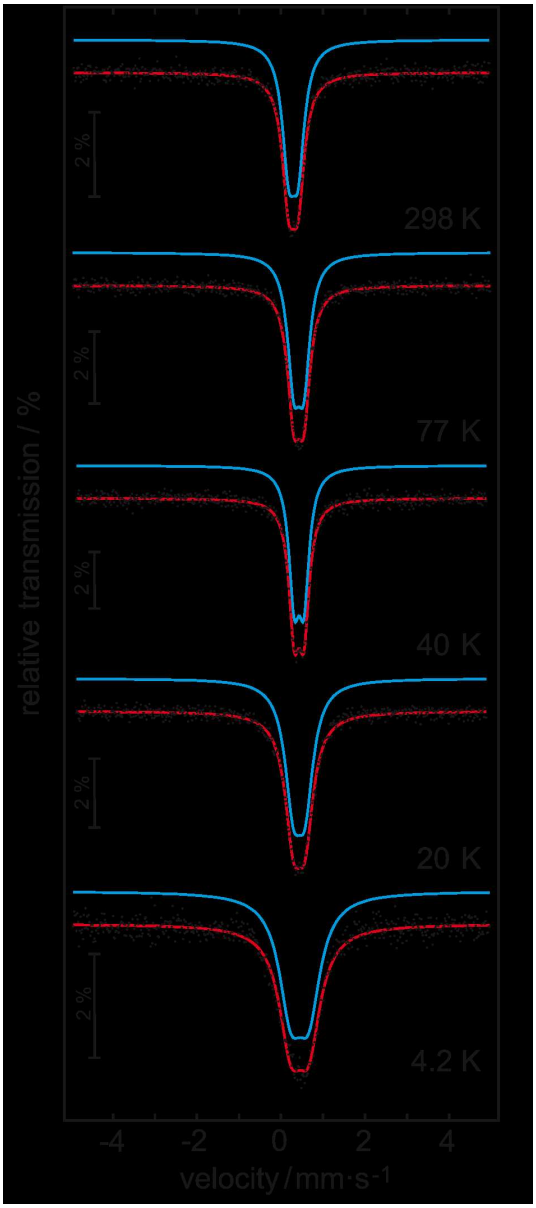

80x180mm (600 x 600 DPI)

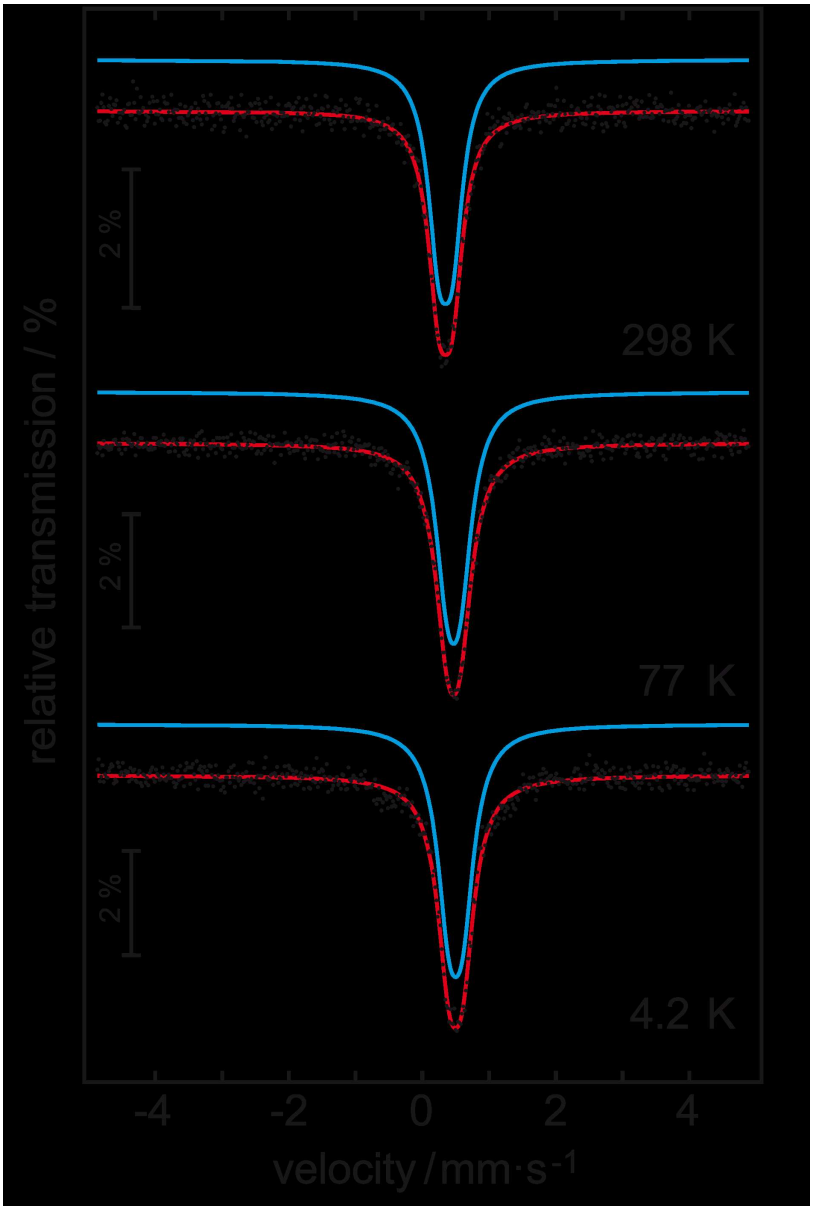

80x118mm (600 x 600 DPI)

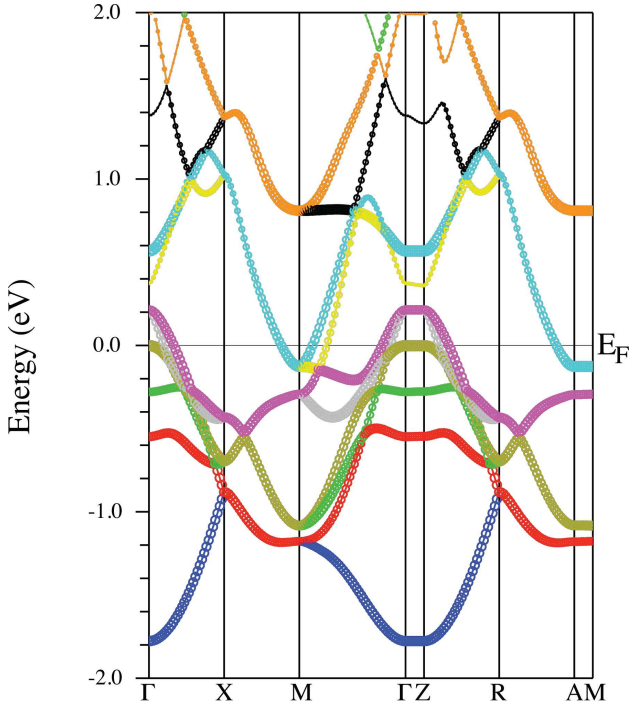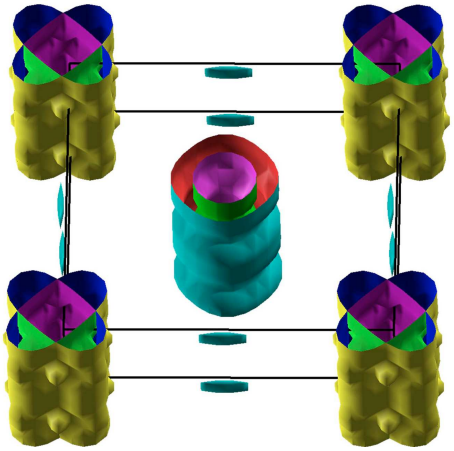
2.0
1.0
0.0
-1.0
-2.0
Energy (eV)
E_F
Γ
X
M
ΓZ
R
AM